ELSEVIER

International Journal of Mass Spectrometry 219 (2002) 23–37

International Journal of Mass Spectrometry

www.elsevier.com/locate/ijms

Charge location on gas phase peptides☆

Herbert H. Hill[a,*], Chandler H. Hill[b], G. Reid Asbury[c], Ching Wu[d], Laura M. Matz[a], Toshiko Ichiye[e]

[a] *Department of Chemistry, Washington State University, Pullman, WA 99164-4630, USA*
[b] *School of Medicine, University of Washington, Seattle, WA 98195, USA*
[c] *Amersham Pharmacia Biotech, 800 Centennial Avenue, Piscataway, NJ 08855, USA*
[d] *Ion Track Instruments, 205 Lowell St., Wilmington, MA 01887, USA*
[e] *Department of Biochemistry and Biophysics, Washington State University, Pullman, WA 99164-4660, USA*

Received 11 September 2001; accepted 22 January 2002

Abstract

Studying biological systems to determine structure has been performed by a number of analytical techniques, including electrospray ionization (ESI)/ion mobility spectrometry (IMS) with mass spectrometry (MS) detection. ESI/IMS/MS enables the determination of gas phase ionic molecular size and can be correlated to computational modeling for structural evaluation. In this study, a molecular modeling program (CHARMm) coupled with a novel method of experimentally determining ion radii with ambient pressure IMS/MS was utilized to determine the charge position on gas phase peptides. Molecular modeling predicted the relative sizes of several isomeric peptides previously separated by IMS in a nitrogen buffer gas, although the modeled radii were smaller than the experimental radii due to the large polarizability of the drift gas. To correct for the polarization of the ambient pressure gas through which the ions migrate in the ion mobility experiment, ionic radii in drift gases of differing polarizability were plotted as a function of drift gas polarizability. To compare with the zero-polarizability ionic radii (*y*-intercept of the linear regression), the modeling experiment mimicked conditions of the actual experiment and the modeled and measured ionic size matched well. Moreover, when all possible charge locations on the peptides were modeled, only one modeled structure matched the experimental data, indicating that the combination of modeled and mobility data can determine charge location on gas phase peptides. (Int J Mass Spectrom 219 (2002) 23–37)

Keywords: Electrospray ionization; Ion mobility spectrometry; Mass spectrometry

1. Introduction

Structural investigation of anhydrous peptide and protein ions in the gas phase, enabled by the development of electrospray ionization (ESI) [1,2] and matrix-assisted laser desorption ionization (MALDI) [3], provides a potentially powerful technique for the investigation of biomolecular structure. Understanding the anhydrous behavior of peptides and proteins may provide fundamental information helpful in the complete characterization of the hydrated forms of biomolecules (see reviews [4,5]).

Several researchers have employed ESI with mass spectrometry (MS) to elucidate biomolecular conformations and structure hydrogen/deuterium exchange

☆ Some of the data presented in this paper was first reported in a symposium entitled "Novel Developments and Applications of Ion Mobility Spectrometry," PITTCON 99, Orlando, Florida, March 7–13, 1999.

* Corresponding author. E-mail: hhhill@wsu.edu

1387-3806/02/$ – see front matter
PII S1387-3806(02)00557-2

experiments [6], proton-transfer experiments [7], and ion beam scattering experiments in which collision cross-section for ions can be determined [8]. The coupling of ESI with ion mobility spectrometry (IMS) and MS detection has enabled further structural studies to be performed due to the technique's inherent ability to measure ionic size [9]. In the past decade, ESI/IMS/MS studies have elucidated differences in protein conformations [4,10–13], folding/unfolding relationships for proteins [14] and peptides [15], and provided understanding of predominating intramolecular interactions [16].

Comparison between computational modeling and experimental IMS results can provide an understanding of the ionic structures that represent the measured ionic collision cross-sections present in the gas phase. The collision cross-section is defined as the average collision integral between the ion and a neutral drift gas [9]. Therefore, computational models need to account for the contribution of the drift gas to the collision cross-section (both due to the mass and interaction with the ion). To reduce drift gas contributions and modeling complexity, helium is typically employed as the buffer gas [17–20]. Several methods have been employed which estimate collision cross-sections from molecular modeling calculations [16,17]. The projection approximation method is the simplest and oldest method [18,19]. More sophisticated methods have been developed as the allowable error for these measurements decreased (exact hard spheres scattering model [20], the trajectory method [21] and the scattering on electron density isosurfaces method [22]). Errors associated with the representation of the ion/drift gas collision integral can create deviations between the experimental and modeled ionic sizes [12,16].

Determination of ionic size from ion mobility data is commonly accomplished by one of two approaches, sub-ambient pressure and ambient pressure IMS. Sub-ambient pressure IMS was first developed to measure ionic size by increasing the pressure in drift mass spectrometers. Today, this approach is still used by several groups measuring ionic size of large molecular weight organic compounds [15,16,18]. To eliminate effects from polarization and other long-range effects of the drift gas, ion size is normally measured in helium drift gas.

Although mobility measurements at atmospheric pressure are more difficult than those obtained using the sub-ambient approach, ambient pressure IMS has several advantages. First, it is possible to use higher voltages and remain in the low field region of operation where size is indirectly proportional to drift time. Second, small errors in pressure measurements do not significantly effect size measurement. And, third, higher resolving powers can be achieved for the same drift length.

Higher resolving powers can also be achieved for drift gases that are more polarizable than He. The reason for this is that for a given IMS instrument and set of operating conditions, drift times are longer in more polarizable drift gases, reducing the pulse width contribution to the total peak width. In addition to longer drift times, drift gases with higher polarizabilities can withstand more voltage before breakdown occurs. As long as ion drift times are sufficiently long to minimize the bandwidth contribution of the initial pulse width, higher voltage across the drift tube results in higher IMS resolving power. With higher resolving power, ion size can be determined to a higher degree of significance.

In order to use higher polarizable drift gases, a new method where experimental ionic radii (based on the rigid sphere model) were measured with IMS in four different drift gases with varied polarizability and a linear relationship between drift gas polarizability and ionic radii was found [23,24]. Based on this approach to account for the drift gas contribution, the zero-polarizability (y-intercept of the linear regression) ionic radii were determined for two biologically relevant peptides and were correlated with molecular dynamics simulations in this study. The determination of the ionic radii without contributions from the drift gas enables direct comparison between molecular models and experimental radii.

Understanding the charge location on biomolecules enables an understanding of folding mechanisms and electrostatic interactions [17]. Although typically

residue basicity is employed as the guideline for assigning charge to specific amino acid residues [25], the addition of two or more charges to a biomolecule complicates this assumption due to Coulombic repulsion forces and self-solvation [17]. The comparison of molecular models with experimental ion mobilities enables assignment of the charge positions. In this study, previously studied isomeric peptides [26] were modeled and charge location on the peptide was determined based on the comparison between the modeled radii and experimentally measured ionic radii.

2. Experimental

2.1. Ion mobility measurements

Collision cross-sections, Ω, were measured from their proportionality to ion mobility drift times in an atmospheric pressure IMS [9] and ion mass was measured using a quadrupole MS coupled in series to the IMS. Both the IMS and the MS have been described previously [27]. The IMS drift tube consists of two regions; a drift region (13.0 cm long) and a desolvation region (7.2 cm long). Both regions were maintained at a constant temperature of 250 °C. A potential of 4.5 kV was applied to the target screen (first ring of the IMS drift tube). The IMS was operated at atmospheric pressure (typically 695 Torr in Pullman, WA) with a counter-current flow of drift gas at a flow rate of 1.2 L min^{-1}. The IMS was interfaced to the ABB Extrel (Pittsburgh, PA) 50-QC quadrupole mass spectrometer via a 40 μm pinhole (pinhole potential +7.9 V) and five electrostatic lenses (−4.9, −20.1, −7.4, −99.9, −23.2 V). The pressure in the ion focusing chamber was maintained at 2.2×10^{-4} Torr and the ion separation chamber was maintained at 1.5×10^{-5} Torr.

Ion mobility measurements were obtained for solutions of kemptide and neurotensin in four different drift gases: He, Ar, N_2 and CO_2. Peptides were sprayed into the IMS from a solution of 47.5% water/47.5% methanol with 5% acetic acid. These solutions were introduced into the IMS at a flow rate of 5 μL min^{-1}.

2.2. Molecular modeling experiments

The molecular modeling experiments were conducted on a commercially available molecular mechanics and dynamics program called CHARMm (Chemistry at Harvard Macromolecular Mechanics), which uses empirical energy functions to describe the forces on atoms in molecules (Molecular Simulations Incorporated, San Diego, CA) [28]. First developed by the research group of Professor Martin Karplus at Harvard University in 1983 [28], the CHARMm molecular dynamics technique implements the Verlet method of numerical integration to relate the mass and acceleration of an atom in the system to the gradient of the potential energy field. This allows the user to generate a realistic picture of a structure's motions and to perform conformational searching at various temperatures. For these experiments, CHARMm Version 24 was run on a 180 MHz Silicon Graphics O2 machine in a UNIX IRIX 6.3 operating system. Structures were imaged with QUANTA 97, a windows-based program by Molecular Simulations Incorporated (San Diego, CA).

The modeling protocol for the isomeric peptides was the following: peptide sequence conformations were generated using CHARMm molecular dynamics and were imaged through the program QUANTA. For each peptide sequence, 10 trial structures were generated in a simulated annealing procedure similar to previous dynamics simulations for ion mobility experiments [29,30]. Straight chain forms of each peptide were minimized, then heated to 1000 K over 5000 ps, equilibrated for 3000 ps, and then cooled to 523 K over 20,000 ps. These cooled structures were equilibrated for 1000 ps and then produced at 523 K for 10,000 ps. This production step traces the motions of the molecule at the designated temperature, generating a set of frames of coordinates that represent the trajectory of the atoms over time. An average structure was obtained from the behavior of the peptides over this period and their final energy was recorded. Averaged structures were then used at the beginning of the annealing cycle in place of the initial straight chain forms and the cycle was repeated until 10 averaged structures

and 10 final energies had been generated. Although a greater number cycles may have produced more accurate structures with lower energies, 10 cycles provided an efficient method for predicting relative mobility behavior of the isomers. The average structure with the lowest final energy was considered the best representation of the peptides conformation during analysis.

The protocol for the neurotensin and kemptide molecules was modified to better reflect experimental conditions (ions generated from liquid phase ionization into a heated drift gas). Each constructed ion was initially subjected to polar conditions similar to an aqueous environment (dielectric constant = 72). In this polar environment, straight chain conformations were minimized, then equilibrated for 1000 ps at 298 K, and allowed to behave dynamically at 298 K for 1000 ps. It is not clear if sampling from a polar environment will alter the sampled structures. Further studies of both modeling methods would identify any slight differences in the sampled structures. However, the polar environment does simulate the experimental conditions better than the method described in the previous section. This process was done once for each peptide and the resultant structures were used as the initial conformation in a following cycle which used non-polar conditions (dielectric constant = 1). In the non-polar environment, the previously generated conformers were minimized, then heated to 523 K over 1000 ps. The structures were equilibrated for 1000 ps and then produced at 523 K for 5000 ps. As with the isomeric peptides, average structures over the 5000 ps of production were generated and the final energies were recorded. These average structures were placed at the beginning of the second, non-polar cycle until 10 average structures and 10 final energies were generated. As with the isomeric peptide experiments, 10 cycles provided an efficient method for establishing charge position. A larger number of cycles may have provided a slightly more accurate structure with lower energies. Again, the average structure with the lowest final energy was chosen as the best representation of peptide conformation for each charge state.

For all of the peptides, once the lowest energy average structure was generated, the radius of gyration (R_g) was calculated from the molecular dynamics trajectory data. R_g is defined as

$$R_g = \sqrt{\frac{1}{N_i}\sum (r_i - r_{cm})^2} \quad (1)$$

where N_i is the number of atoms in the ion, $r_i - r_{cm}$ is the distance between the atom 'i' and the center of mass for the ion. The radius of gyration is considered to be an average radius for the ion at 523 K (the operating temperature for the IMS drift tube) in the absence of any other molecules.

2.3. Calculations

The reduced mobility values reported were calculated based on the following equation:

$$K_o = \left(\frac{L^2}{Vt_d}\right)\left(\frac{273}{T}\right)\left(\frac{P}{760}\right) \quad (2)$$

where L is the drift region length (13.0 cm), V the drift voltage, T the effective temperature in the drift region (523 K), and P is the pressure in the drift region.

The average ion collision cross-section (Ω) was calculated from the following equation [9]:

$$\Omega = \left(\frac{3}{16N}\right)\left(\frac{2\pi}{\mu kT}\right)^{1/2}\left(\frac{zeVt_d}{L^2}\right) \quad (3)$$

where z is the number of the charges on the ion, e the charge of one proton, N the number density of the drift gas, μ [$=mM/(m+M)$] is the reduced mass of an ion (m) and the neutral drift gas (M), and k is Boltzmann's constant.

For the purpose of this discussion, ion radii were determined using the hard sphere model in which

$$\Omega = \pi(r_i + r_g)^2 \quad (4)$$

where r_i is the intrinsic radius of the ion and r_g is the radius of the neutral drift gas. As the polarizability of a drift gas increases, the effective radii of the drift gas is going to increase. This increase will be dependent

Table 1
Polarizability and calculated radii of drift gases

Ion mobility drift gas	Radius (Å)[a]	Polarizability ($\times 10^{-24}$ cm^3)[b]
Helium	1.03	0.205
Argon	1.67	1.641
Nitrogen	1.73	1.740
Carbon dioxide	2.02	2.911

[a] As calculated in [23].
[b] As tabulated in [32].

on both the drift gas and the specific ion. The effective drift gas radii (r_g) can be thought to have two contributions

$$r_g = r_p + r_v \quad (5)$$

where r_p is that portion of the drift gas radius which was due to the increase in the drift gas radii because of the interaction with the ion during the collision and r_v is the actual drift gas radius in the absence of other molecules (defined as the Van der Waals radius). The Van der Waals radii used for the neutral drift gases in these experiments are given in Table 1. For all of the experimentally reported radii, Eq. (3) was employed to calculate the collision cross-section. Substitution of Eq. (5) into Eq. (4) and rearrangement of Eq. (4) results in the following equation:

$$r_i + r_p = \sqrt{\frac{\Omega}{\pi}} - r_v \quad (6)$$

Eq. (6) was utilized to determine the experimentally measured radius, defined as the sum of the ion radii and polarizable radii contribution ($r_e = r_i + r_p$)

2.4. Method of zero-polarizability radii

For direct comparison between the experimental results and the molecular modeled structures, the intrinsic ion radii was calculated by removing r_p, the contribution of the drift gas from the experimentally measured radius (r_e), labeled the zero-polarizability method. In this method, the mobility and collision cross-section values for a given ion were determined in four drift gases and the r_e values were calculated in each drift gas by Eq. (6). The r_e values were linearly correlated with the drift gas polarizability. The linear correlation between r_e and drift gas polarizability has been demonstrated in previous studies [23,24]. In this empirical correlation, it is assumed that the ionic radii does not change significantly in the presence of different drift gases, but rather that the apparent drift gas radii (r_g) increases with increased polarizability. With this assumption, the intrinsic ionic radii r_i is defined as the r_e value where there is no contribution from the drift gas (i.e., $r_p = 0$); i.e., the y-intercept for the linear relationship. For both the zero-polarizability intrinsic ion radii and the computationally derived radii of gyration, we are assuming that the structures should be similar because they are both radii essentially under vacuum conditions. Therefore, we feel that a direct comparison between these two ionic radii is valid.

Table 2
Experimental and modeled radii for six isomeric peptides

Doubly charged peptide ion sequence	MW (Da)	Collision cross-section (Å^2)	Ion radius (Å)	Modeled radius (Å)
SerH$^+$–Asp–Gly–ArgH$^+$–Gly	492.5	222	6.7	6.3
GlyH$^+$–ArgH$^+$–Gly–Asp–Ser	492.5	211	6.5	5.3
SarH$^+$–ArgH$^+$–Gly–Asp–Ser–Pro	603.6	228	6.8	4.0
GlyH$^+$–ArgH$^+$–Gly–Asp–Thr–Pro	603.6	233	6.9	4.6
Leu–ArgH$^+$–ArgH$^+$–Ala–Ser–Leu–Gly	773.9	281	7.7	6.4
Leu–ArgH$^+$–ArgH$^+$–Ala–Ser–Val–Ala	773.9	280	7.7	6.5

Experimental values were obtained from [24] and were performed with nitrogen as the drift gas. Both modeled and experimental radii were calculated according to equation where the nitrogen was approximated to be equal to 1.73 Å.

3. Results and discussion

3.1. Isomeric peptide models

The distinction between isomeric peptides is difficult to perform by MS alone but has been shown to be easily achieved with high resolution IMS instruments [26]. Based on previous IMS studies where ion mobility separations of isomeric peptides were demonstrated [26], modeling experiments for three isomeric peptide pairs; (1) Ser–Asp–Gly–Arg–Gly (SG)/Gly–Arg–Gly–Asp–Ser (GS); (2) Sar–Arg–Gly–Asp–Ser–Pro (SP)/Gly–Arg–Gly–Asp–Thr–Pro (GP), and (3) Leu–Arg–Arg–Ala–Ser–Leu–Gly (LG)/Leu–Arg–Arg–Ala–Ser–Val–Ala (LA) were performed. The ion mobility data for these ions were taken from [26]. The experimental collision cross-section values, the experimentally measured radii (r_e), and modeled radii of gyration for the six peptides are listed in Table 2.

For the first peptide pair which was the inverse amino acid sequence, SG and GS, both singly and doubly charged gas phase ions were observed. The singly charged ions were not separated by IMS and both produced an experimental collision cross-section of 184.5 Å^2 and measured radii of 5.94 Å. The doubly charged inverse isomeric ions were completely resolved, having experimental cross-sections in nitrogen of 222 Å^2 (r = 6.7 Å) for SG and 211 Å^2 (r = 6.5 Å) for GS. In Fig. 1, both the ionic structures and ionic radii of gyration determined from the molecular modeling for the doubly charged ions are shown (6.3 Å for SG and 5.3 Å for GS). For both peptides, the modeled radii of gyration were significantly smaller than the experimentally measured radii. This result was expected since the molecular models were generated without the influence of a drift gas while the experimentally measured radii were obtained in nitrogen and contain a contribution from the drift gas (r_p). The model does however predict that the doubly charged SerH$^+$–Asp–Gly–ArgH$^+$–Gly (SG) was elongated and maintained a stretched structure due to separation of the two protonated sites. The charge repulsion of the two adjacent charged sites for GlyH$^+$–ArgH$^+$–Gly–Asp–Ser (GS) caused the backbone from the last three amino acids to fold around in order to stabilize the charge on the N-terminal glycine (see Fig. 1). While the modeled radii of gyration

Table 3
Experimental ion mobility measurements for kemptide and neurotensin in four drift gases

Ion	MW	G_d	R_r	t_d	K_o	Ω	r_i
Kemptide 2+ $(M + 2H)^{2+}$	773	He	155.4	14.0	3.51	231.4	6.85
	773	N_2	42.7	25.0	1.10	285.8	7.81
	773	Ar	19.7	27.8	0.98	267.9	7.57
	773	CO_2	9.8	36.1	0.76	332.5	8.27
Kemptide 1+ $(M + H)^+$	773	He	16.8	7.7	1.96	208.1	6.41
	773	N_2	2.6	45.2	0.61	258.2	7.34
	773	Ar	2.9	50.2	0.54	241.9	7.11
	773	CO_2	0.7	61.8	0.44	284.5	7.50
Neurotensin 3+ $(M + 3H)^{3+}$	1674	He	100	9.5	2.86	425.4	9.91
	1674	N_2	10.7	29.3	0.94	492.3	10.91
	1674	Ar	4.9	33.1	0.82	472.6	10.41
	1674	CO_2	1.3	41.4	0.66	564.1	11.40
Neurotensin 2+ $(M + 2H)^{2+}$	1674	He	47.6	12.7	2.16	376.9	9.23
	1674	N_2	10.7	37.7	0.73	426.6	9.92
	1674	Ar	11.6	42.8	0.64	406.7	9.71
	1674	CO_2	2.8	51.4	0.53	466.8	10.17

MW: molecular weight (amu); G_d: drift gas; R_r: relative peak height response; t_d: drift time (ms); K_o: reduced mobility constant (cm^2 V^{-1} s^{-1}); Ω: collision cross-section (Å^2); r_i: hard sphere ion radius (Å).

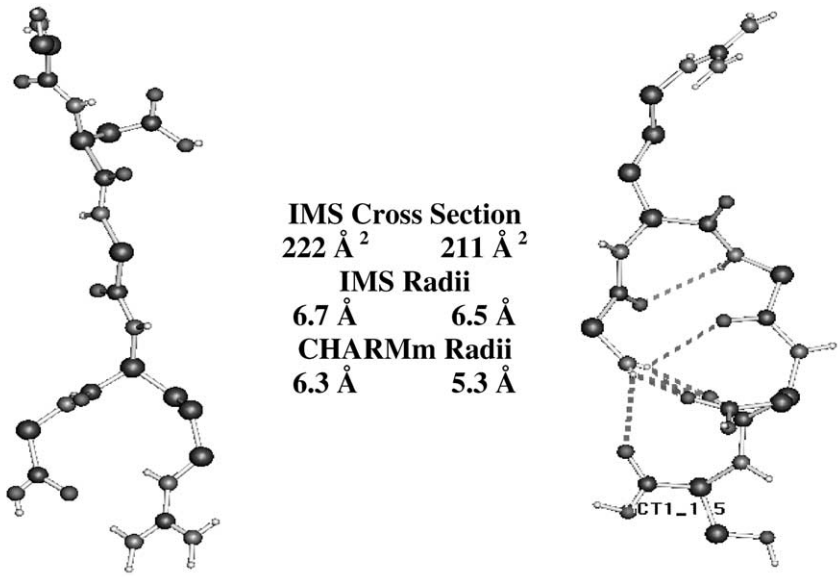

Fig. 1. Minimized molecular models of gas phase inverse-sequence isomeric peptide ions. Collision cross-section values were obtained from [24], experimental ionic radii were calculated from Eq. (3).

and experimentally measured radii did not match, the relative radii predicted separation.

As with the inverse isomeric pair, Sar–Arg–Gly–Asp–Ser–Pro (SP) and Gly–Arg–Gly–Asp–Thr–Pro (GP), produced both singly and doubly charged gas phase ions. In this second pair, the methyl group on sarcosine was moved to the serine, thus converting sarcosine to glycine and serine to threonine. Again, the singly charged ions could not be separated, producing a cross-section of 210 and 211 $Å^2$, respectively. The doubly charged isomers could be separated however, having cross-sections of 227 $Å^2$ for $SarH^+$–$ArgH^+$–Gly–Asp–Ser–Pro and 233 $Å^2$ for $GlyH^+$–$ArgH^+$–Gly–Asp–Thr–Pro. Fig. 2 illustrates the result of the molecular modeling for the doubly charged isomeric peptides. As shown in Table 3, the modeled ion radii of gyration were again significantly smaller than the experimentally measured radii (6.8 Å/4.0 Å for SP and 6.9 Å/4.6 Å for GP), however, the peptide with the smallest experimental radii also produced the smallest modeled radii of gyration.

For the methyl substituted isometric pair, Leu–Arg–Arg–Ala–Ser–Leu–Gly and Leu–Arg–Arg–Ala–Ser–Val–Ala, only doubly charged ions were observed and the structures were not sufficiently different to be separated. The only difference between these two isomers was the methyl group at the non-charged, C-terminal end of the peptide. For modeling, it was not clear where the charges were located on the peptide since there were three possible charge sites but only two charges. For this modeling experiment, charge locations were selected on relative basicity and the two protons were attached to the Arg groups. Fig. 3 illustrates a similar structure for both of these isomers in which the Arg group nearest the N-terminal end of the peptide is stabilized with the carbonyl of the N-terminal amino acid and the charged Arg group nearest the C-terminal end is stabilized by interactions with carbonyl groups on the C-terminal end of the peptide. The dominating factor is the electrostatic repulsion of the two charged Arg groups.

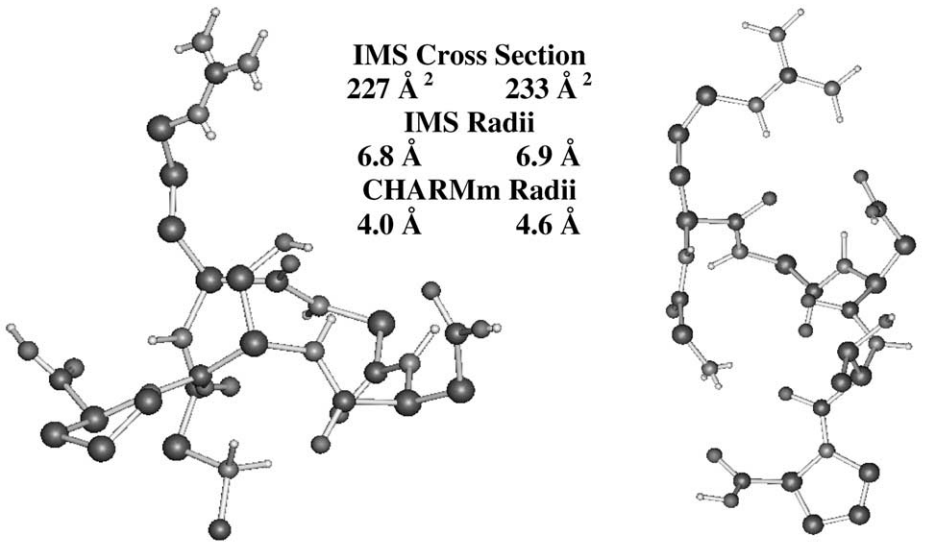

Fig. 2. Minimized molecular models of primary and secondary amine isomeric peptide ions. Collision cross-section values were obtained from [24], experimental ionic radii were calculated from Eq. (3).

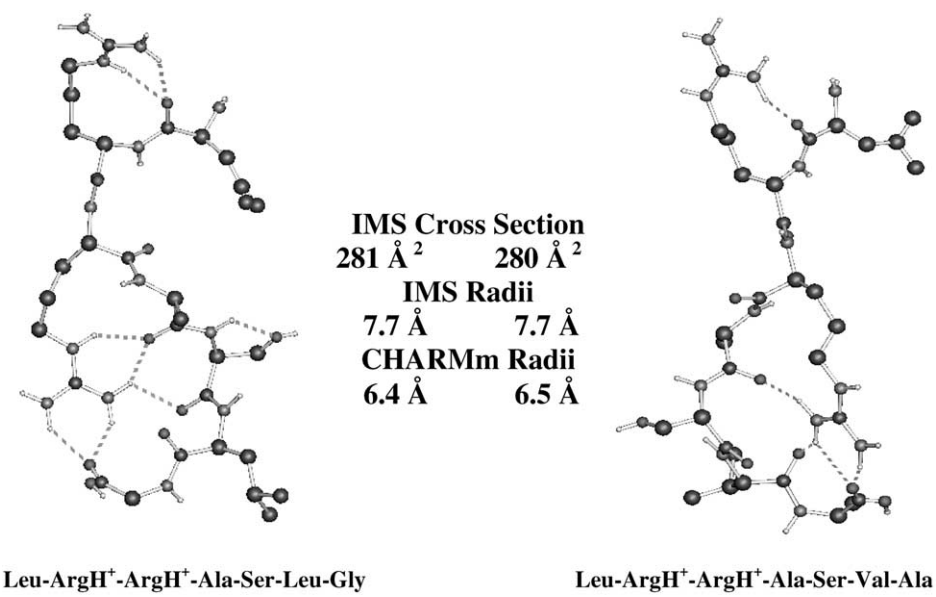

Fig. 3. Minimized molecular models of R-group modified isomeric peptide ions. Collision cross-section values were obtained from [24], experimental ionic radii were calculated from Eq. (3).

Although the calculated R_g and experimentally measured nitrogen radii for each peptide pair can not be directly compared, the computational models correctly described the experimental separation of the each peptide pair. This is a qualitative approach to understanding the separation characteristics and the molecular structures that dictate differences in the mobilities. It is important to point out that this is only valid when each ion is analyzed separately and each mobility is determined independently. For some ions, the relative collision cross-sections will differ in a polarizable drift gas from the relative sizes of each ion without contribution from the drift gas.

3.2. Ion mobility size measurements of neurotensin and kemptide in different drift gases

As already mentioned, modeled radii of gyration were significantly smaller than the experimental radii in all cases. The reason for this was that the modeled R_g values were obtained without accounting for the influence of the drift gas while the experimentally measured values were obtained in a relatively polarizable drift gas, nitrogen. The experimental radii were actually due to both the intrinsic ion radii (r_i) and the increase in the drift gas radii due to the polarization of the drift gas molecule (r_p). To experimentally correct for the effect of the polarizability of the drift gas, ionic radii were determined in drift gases of different polarizability. The experimentally measured ionic radii were plotted as a function of drift gas polarizability [23,24] and the ion radii at the zero-polarizability intercept (*y*-intercept for the linear regression) were used to compare with modeled R_g values. Table 1 lists the drift gases used in this experiment along with their Van der Waals radii and polarizability.

Fig. 4 shows the ion mobility spectra obtained for kemptide in the different drift gases. In all drift gases, both the singly and doubly charged ions were observed but the doubly charged ions were the primary species observed. Fig. 5 shows the ion mobility spectra obtained for neurotensin in the different drift gases. For neurotensin, only the $(M + 2H)^{2+}$ and $(M + 3H)^{3+}$ ions were observed. Table 3 list the drift

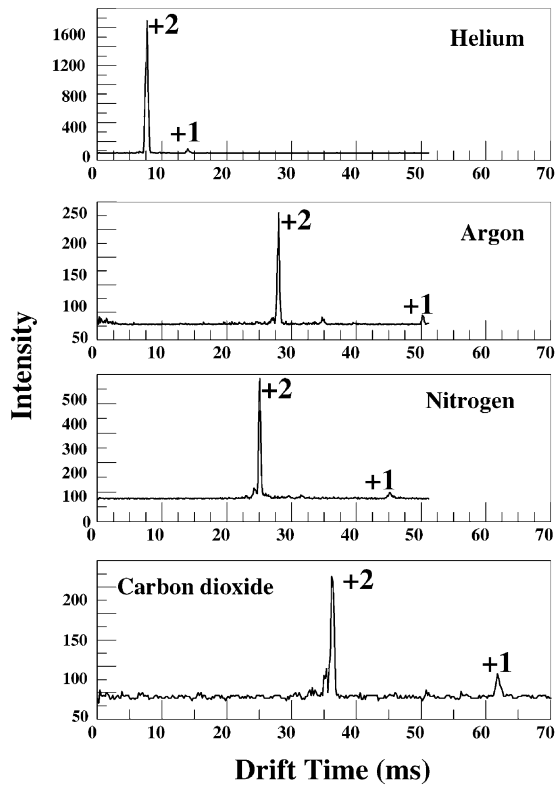

Fig. 4. Ion mobility spectra of kemptide in four different drift gases.

times, mobility values and collision cross-sections calculated for these four ions.

Fig. 6 shows the experimentally measured radii spectra plotted as a function of the polarizability of the drift gasses for each of the kemptide and neurotensin ions observed in the ion mobility. From the graph, it is clear to see that the measured radii varied linearly with polarizability of the drift in the following manner:

$$r_e = m\alpha + r_i \quad (6)$$

where m is the slope of the line and α is the polarizability of the drift gas. In addition, it appears that the slope of the line is a function of the charge density of the ion. From Fig. 6, the triply charged ion for neurotensin had a steeper slope than the doubly charged ion and the doubly charged ion of kemptide

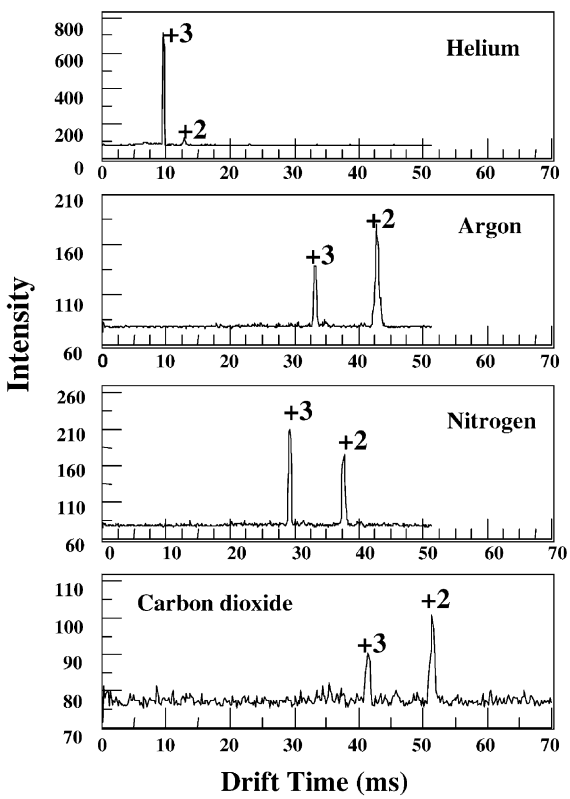

Fig. 5. Ion mobility spectra of neurotensin in different drift gases.

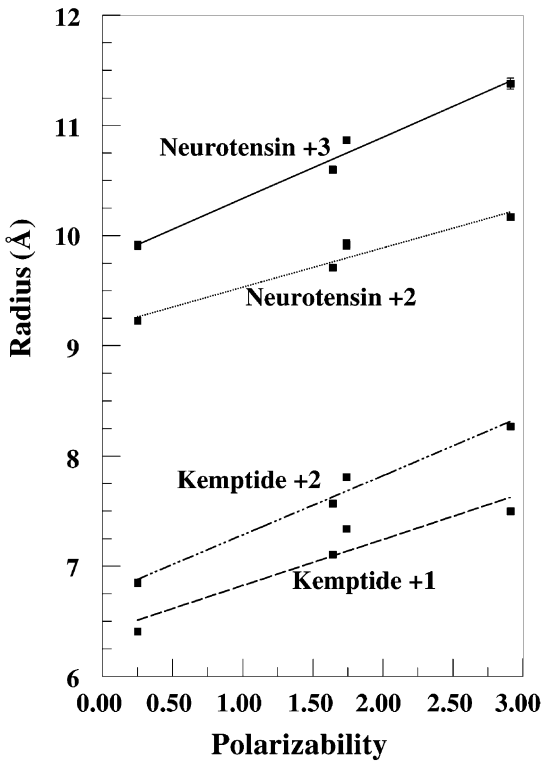

Fig. 6. Calculated ion radii as a function of drift gas polarizability for kemptide and neurotensin. The slopes for the higher charged ions for each peptide have a greater slope than their smaller charged counterparts.

had a steeper slope than the singly charged ion. In other studies, we have observed similar phenomenon [23] where small singly charged ions have a steeper slope than peptide ions.

In all cases, the ionic radii in He, Ar, and CO_2 fell on a line while the radii measured in N_2 always fell a little above the line. One explanation for this phenomenon is that N_2 was the only drift gas that had a significant quadrupole moment. Thus, long-range interactions between the gas and ion were larger that predicted based on polarizability alone.

3.3. Molecular modeling measurements

Experimental results indicated that only the $(M + H)^+$ and $(M + 2H)^{2+}$ ions were generated by the electrospray process for kemptide (Leu–Arg–Arg–Ala–Ser–Leu–Gly) even though there were three basic sites (N-terminal leucine and the two arginines) on the peptide where a proton could attach. Similarly, neurotensin (Glu–Leu–Tyr–Glu–Asn–Lys–Pro–Arg–Arg–Pro–Tyr–Ile–Leu) can accept four protons, one on the N-terminal glutamine, one on the lysine, and two on the arginines. However, experimental results indicated that only the $(M + 2H)^{2+}$ and $(M + 3H)^{3+}$ ions were observed after electrospray. For modeling the peptides, this presents a problem.

When faced with the problem of where to locate charge on peptides, modelers in the past have selected the most basic sites [25]. While this approach seems reasonable, other considerations may also be important such as proximity to other charges and intramolecular stabilization of the charge, for example [17]. Thus,

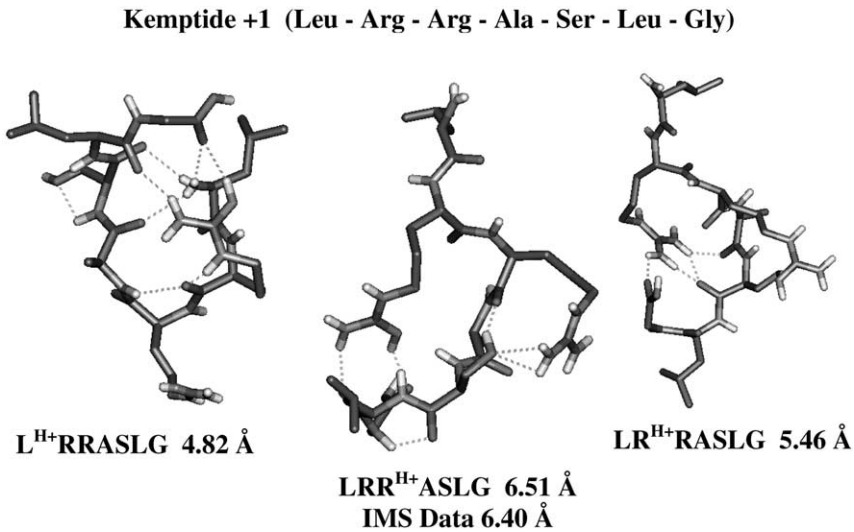

Fig. 7. Minimized molecular models of singly charged kemptide at all possible charge sites.

in these experiments, we modeled all possible charge sites.

Modeling results for the singly charged kemptide ion are shown in Fig. 7. The position of the proton is denoted by the superscript H^+. The smallest configuration occurred when the proton was placed on the N-terminal amino group of the peptide. Here, the peptide folded back on itself to stabilize the proton with the carbonyl groups of the C-terminal end of the peptide producing a radius of gyration of 4.82 Å. When the proton was placed on the adjacent arginine, the C-terminal end of the peptide folded around the arginine group, leaving the N-terminal amino acid free, sticking out of the folded portion of the peptide and producing an ion with a radius of gyration of 5.46 Å. Placing the proton on the second arginine from the N-terminal end of the peptide resulted in the largest R_g. In this structure, placing the charge near to the C-terminal end prevented the peptide from folding as tightly, producing the largest of the three structures with a radius of gyration of 6.51 Å. Thus, placing the charge on the N-terminal end produced the smallest configuration, which increased in size as the charge was placed nearer to the center of the peptide. Which of these configurations was the most likely to actually occur in the gas phase?

From Fig. 4, it is clear that only one singly charged peptide ion was observed in the ion mobility spectrum of kemptide. If all three modeled stable configurations had been produced in the electrospray ionization process, then three ion mobility peaks corresponding to R_g values of 4.82, 5.46, and 6.51 Å would have been observed. The ion mobility spectrometer used in this study had a resolving power of 80, which is capable of separating ions with radii differences as small as 0.1 Å. Thus, the conditions used in this study were sufficient to detect the presence of three stable singly charged kemptide ions but only one was observed.

Was this single ion mobility peak the result of some dynamic, proton-transfer process that occurred during in the gas phase during the ion migration process? If proton-transfer reactions were occurring during the migration process, the measured radius of gyration would be some weighted average of those radii calculated for the three modeled ion structures, the average radius of gyration for the three modeled structures would be 5.60 Å if all conformations were weighted equally. The intrinsic ion radius that was actually measured with these ion mobility experiments was 6.40 Å,

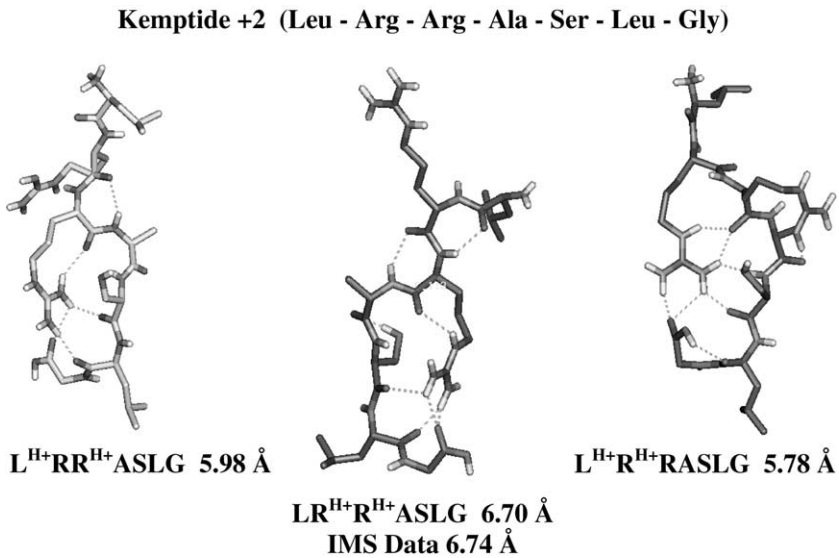

Fig. 8. Minimized molecular models of doubly charged kemptide at all possible charge sites.

well separated from the average of all conformations. In fact, the measured ion radius was only slightly less than the radius of gyration of 6.51 Å determined from the conformation in which the proton was positioned on the arginine that was in the third amino acid position. From this near match of measured and modeled ionic radii, it would seem reasonable that the proton was attached to the arginine in the third position and that intramolecular gas phase proton-transfer reactions did not occur during the migration of the ion through the drift region of the spectrometer.

Similarly, Fig. 8 shows the three modeled configurations for the three possible proton positions in the doubly protonated kemptide. Again, when protons were attached to the N-terminal amino acid, the peptide folded tightly to produce radii of gyration of 5.78 and 5.98 Å. When the two protons were attached to the two arginines in the second and third positions, the peptide was in the more unfolded state with a radius of gyration of 6.70 Å. The actual intrinsic ion radius determined from ion mobility experiments was 6.74 Å, indicating that the stable gas phase ion structure of the $(M + 2H)^{2+}$ kemptide ion occurred when the protons were attached to the two arginines.

For neurotensin, only the $(M + 2H)^{2+}$ and $(M + 3H)^{3+}$ ions were observed in the IMS even though there were four possible protonation sites in the peptide. Modeling all of the possible proton-positions in each ion was more challenging since there were six possible positions in the $(M+2H)^{2+}$ ion and four possible positions in the $(M + 3H)^{3+}$ ion. The six minimum energy conformations modeled along with their average radii of gyration for the six possible proton positions for the doubly protonated neurotensin are presented in Table 4. In this case, the intrinsic ion

Table 4
Calculated radii of gyration values for six possible doubly charged ions of neurotensin (amino acid sequence is: E_1LYENKPR_1R_2 PYIL)

Charge location on amino acids in simulated structure	Calculated radius of gyration (Å) for simulated structure
E_1R_1	8.15
KR_1	10.13
E_1R_2	11.51
E_1K	11.84
KR_2	8.70
R_1R_2	9.74

Experimental zero-polarizability IMS radii was determined to be 9.17 Å.

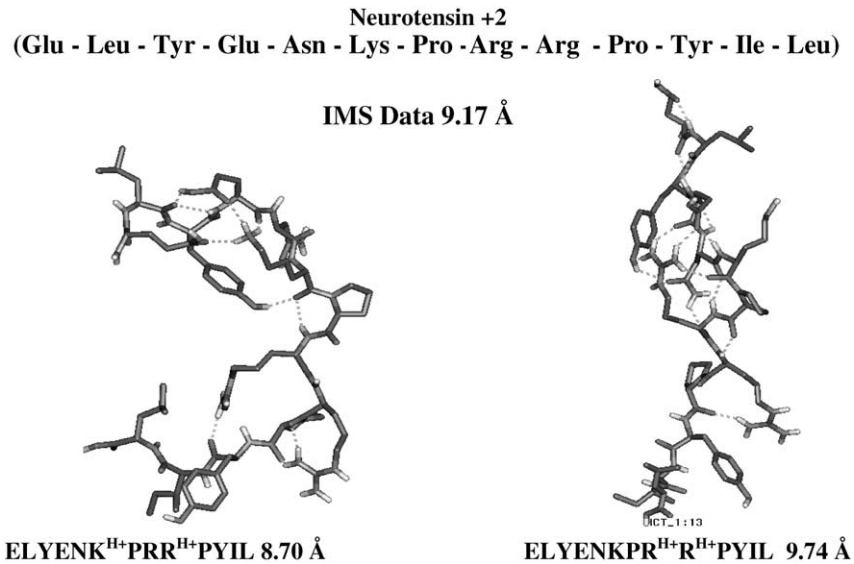

Fig. 9. Minimized molecular models of doubly charged neurotensin at all possible charge sites.

radius was 9.17 Å for the peak observed in the ion mobility spectrum did not match any of the modeled radii of gyration. Instead, it fell in between the radii of gyration for the doubly protonated peptide in which the protons were located on the sixth position lysine and the ninth position arginine, 8.70 Å, and the one in which the protons were located on the eighth position arginine and the ninth position arginine, 9.74 Å (see Fig. 9). The average of these two peptides was 9.22 Å, suggesting that these two conformations were in dynamic equilibrium during the ion mobility migration process.

In both structures, one of the protons was present on the ninth amino acid, arginine. The second proton was present on either the eight position arginine (R_g = 9.74 Å) or on the sixth amino acid, lysine (R_g = 8.70 Å). One plausible explanation for the discrepancy between the intrinsic ion radius and the radii of gyration is that the ion was actually interconverting between the two structures already described. In Fig. 9, the modeled representation for each of these structures are shown. In both structures, an upper and lower pocket, each containing one of the two protons, are seen. In each pocket, the proton is hydrogen bonded to the surrounding functional groups from the adjacent amino acids. In both structures, the protons reside in approximately the same area within the ion, and the difference in the structures is the rotation of either the sixth lysine or the eighth arginine to associate with the proton. Therefore, it seems possible that with the thermal energy provided by the ion mobility experiment, the lysine and arginine could flip back and forth within the experiment and that the measured mobility for the doubly charged ion is actually a combination of these two different conformations. One approach to discern the presence of interchangeable conformers is by decreasing the drift tube temperature and observing the predominant peaks as the thermodynamic energy of the system is decreased. Researchers typically perform variable temperature experiments in order to elucidate multiple conformations in biomolecules [31] and a similar approach for neurotensin would be expected to corroborate the suggested conversion between the two peptide structures.

Four proton positions were possible for the triply protonated neurotensin ion and their minimum energy models are shown in Fig. 10 along with their respective

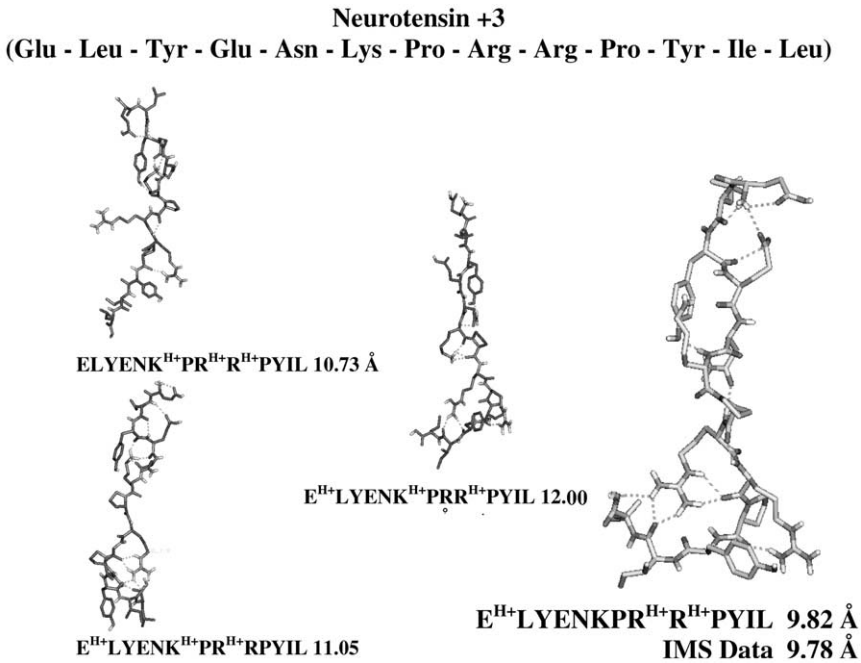

Fig. 10. Minimized molecular models of triply charge neurotensin at all possible charge sites.

radii of gyration. As with the kemptide ion models, the ion mobility measured radius of 9.78 Å matched only one of the modeled radii. In this case, the most stable conformation occurred when the protons were located on the N-terminal amino acid, the eighth position arginine and the ninth position arginine, producing a radius of gyration of 9.82 Å. This was the only case we observed where the proton was attached to the N-terminal amino acid.

4. Conclusions

Molecular dynamics simulations provided accurate three-dimensional models of possible gas phase ionic structures for three isomeric peptide pairs. Although the exact values of the modeled and experimental radii differed, a relative comparison between the modeled and experimental values provided an understanding of the molecular shapes that were associated with the ion mobility measurements. Interestingly, the molecular models for the doubly charged ions of each isomeric peptide pair provided not only relative shapes but also showed the intramolecular interactions which occur to stabilize the charge.

By using the varied drift gas method to determine the zero-polarizability ion radii, the modeled and experimental radii could be directly compared. It was possible to predict protonation sites of gas phase peptides. From the limited number of examples presented here, it appears that most protonation sites are localized and do not undergo intramolecular protonation reactions in the gas phase. Nevertheless, gas phase ion conformations exist where intramolecular proton-transfer reactions can occur. Under these conditions the ion mobility data produce intermediate size information.

Acknowledgements

The project was supported in part by Washington State University Alcohol and Drug Abuse Program and a NIDA Grant (IR03DA1192301).

References

[1] J.B. Fenn, N. Mann, C.K. Meng, S.F. Wong, Mass Spectrom. Rev. 9 (1990) 37.

[2] (a) J. Gieniec, H.L. Fox, D. Teer, M. Dole, in: Proceedings of the 20th ASMS Conference on Mass Spectrometry Allied Topics, 1972, p. 267 (Abstracts);
(b) M. Dole, C.V. Gupta, L.L. Mack, K. Nakamae, Polym. Prepr., Am. Chem. Soc., Div. Polym. Chem. 18 (1977) 188.

[3] F. Hillenkamp, M. Karas, R.C. Beavis, B.T. Chait, Anal. Chem. 63 (1991) 1193A.

[4] (a) D.E. Clemmer, M.F. Jarrold, J. Mass Spectrom. 32 (1997) 577;
(b) C.S. Hoaglund-Hyzer, A.E. Counterman, D.E. Clemmer, Chem. Rev. 99 (1999) 3037.

[5] M.F. Jarrold, Ann. Rev. Phys. Chem. 51 (2000) 179.

[6] (a) B.E. Winger, K.J. Light-Wahl, A.L. Rockwood, R.D. Smith, J. Am. Chem. Soc. 114 (1992) 5897;
(b) D. Suckau, Y. Shi, S.C. Beu, M.W. Sneko, J.P. Quinn, R.M. Wampler, F.W. McLafferty, Proc. Natl. Acad. Sci. U.S.A. 90 (1993) 790;
(c) T.D. Wood, R.A. Chorush, F.M. Wampler, D.P. Little, P.B. O'Connor, F.W. McLafferty, Proc. Natl. Acad. Sci. U.S.A. 92 (1995) 2451.

[7] D.S. Gross, P.D. Schnier, S.E. Rodriguez-Cruz, C.K. Fagerquist, E.R. Williams, Proc. Natl. Acad. Sci. U.S.A. 93 (1996) 3143.

[8] (a) T.R. Covey, D.J. Douglas, J. Am. Soc. Mass Spectrom. 4 (1993) 616;
(b) B.A. Collings, D.J. Douglas, J. Am. Chem. Soc. 118 (1996) 4488;
(c) K.A. Cox, R.K. Julian, R.G. Cooks, R.E. Kaiser, J. Am. Soc. Mass Spectrom. 5 (1994) 127.

[9] H.E. Revercomb, E.A. Mason, Anal. Chem. 47 (1975) 970.

[10] Y.H. Chen, Electrospray Ionization–Ion Mobility Spectrometry, Ph.D. Thesis Dissertation, Washington State University, Pullman, WA, 1994.

[11] S. Ideue, K. Sakamoto, K. Honma, D.E. Clemmer, Chem. Phys. Lett. 12 (2001) 885.

[12] K.B. Shelimov, D.E. Clemmer, R.R. Hudgins, M.F. Jarrold, J. Am. Chem. Soc. 119 (1997) 2240.

[13] R.W. Purves, D.A. Barnett, B. Ells, R. Guevremont, J. Am. Soc. Mass Spectrom. 12 (2001) 894.

[14] S.J. Valentine, D.E. Clemmer, J. Am. Chem. Soc. 119 (1997) 3558.

[15] A.E. Counterman, D.E. Clemmer, J. Am. Chem. Soc. 123 (2001) 1490.

[16] T. Wyttenbach, G. von Helden, M.T. Bowers, J. Am. Chem. Soc. 118 (1996) 8355.

[17] Y. Mao, J. Woenckhaus, J. Kolafa, M.A. Ratner, M.F. Jarrold, J. Am. Chem. Soc. 121 (1999) 2712.

[18] E. Mack Jr., J. Am. Chem. Soc. 47 (1925) 2468.

[19] (a) M.F. Jarrold, V.A. Constant, Phys. Rev. Lett. 67 (1992) 2994;
(b) G. von Helden, M.T. Hsu, N. Gotts, J. Phys. Chem. 97 (1993) 8182;
(c) D.E. Clemmer, J.M. Hunter, K.B. Shelimov, M.F. Jarrold, Nature 372 (1994) 248.

[20] A.A. Shvartsburg, M.F. Jarrold, Chem. Phys. Lett. 261 (1996) 86.

[21] M.F. Mesleh, J.M. Hunter, A.A. Shvartsburg, G.C. Schatz, M.F. Jarrold, J. Phys. Chem. A 100 (1996) 16082.

[22] A.A. Shvartsburg, B. Liu, M.F. Jarrold, K.M. Ho, J. Chem. Phys. 112 (2000) 4517.

[23] G.R. Asbury, H.H. Hill, Anal. Chem. 72 (2000) 580.

[24] L. Beegle, I. Kanik, L. Matz, H.H. Hill, Anal. Chem. 73 (2001) 3028.

[25] H.D. Blatt, P.E. Smith, B.M. Pettitt, J. Phys. Chem. 101 (1997) 7628.

[26] C. Wu, W.F. Siems, J. Klasmeier, H.H. Hill, Anal. Chem. 72 (2000) 391.

[27] C. Wu, W.F. Siems, G.R. Asbury, H.H. Hill, Anal. Chem. 70 (1998) 4929.

[28] B.R. Brooks, R.E. Bruccoleri, B.D. Olafson, D.J. States, S. Swaminathan, M. Karplus, J. Comput. Chem. 4 (1983) 187.

[29] T. Wyttenbach, J.E. Bushnell, M.T. Bowers, J. Am. Chem. Soc. 118 (1996) 8355.

[30] M.F. Jarrold, E.C. Honea, J. Am. Chem. Soc. 114 (1992) 459.

[31] Y. Mao, J. Woenckhaus, J. Kolafa, M.A. Ratner, M.F. Jarrold, J. Am. Chem. Soc. 121 (1999) 2712.

[32] D.R. Lide (Ed.), CRC Handbook of Chemistry and Physics, 70th Edition, CRC Press, Boca Raton, FL, 1989.